Developmental and sexual dimorphic atlas of the prenatal mouse external genitalia at the single-cell level

Ciro Maurizio Amato[a] and Humphrey Hung-Chang Yao[a,1]

[a]Reproductive Developmental Biology Group, National Institute of Environmental Health Sciences, Research Triangle Park, NC 27709

Edited by Thomas E. Spencer, University of Missouri, Columbia, MO, and approved April 27, 2021 (received for review March 2, 2021)

Birth defects of the external genitalia are among the most common in the world. Proper formation of the external genitalia requires a highly orchestrated process that involves special cell populations and sexually dimorphic hormone signaling. It is clear what the end result of the sexually dimorphic development is (a penis in the male versus clitoris in the female); however, the cell populations involved in the process remain poorly defined. Here, we used single-cell messenger RNA sequencing in mouse embryos to uncover the dynamic changes in cell populations in the external genitalia during the critical morphogenetic window. We found that overall, male and female external genitalia are largely composed of the same core cellular components. At the bipotential stage of development (embryonic day or E14.5), few differences in cell populational composition exist between male and female. Although similar in cell population composition, genetic differences in key sexual differentiation developmental pathways arise between males and females by the early (E16.5) and late (E18.5) differentiation stages. These differences include discrete cell populations with distinct responsiveness to androgen and estrogen. By late sexual differentiation (E18.5), unique cell populations in both male and female genitalia become apparent and are enriched with androgen- and estrogen-responsive genes, respectively. These data provide insights into the morphogenesis of the external genitalia that could be used to understand diseases associated with defects in the external genitalia.

sexual dimorphism | penis | clitoris | genital defects | single-cell sequencing

External genitalia are the quintessential sexually dimorphic organs, which represent sex differences in both anatomy and function. This anatomical diversification between the sexes is derived from the genital tubercle, a bipotential progenitor indistinguishable between male and female embryos before the onset of sexual differentiation (1). In both sexes, the genital tubercle undergoes dramatic changes in morphology during embryonic development, leading to the formation of distinct structures including glans and preputial swelling. In both male and female genitalia, the glans is a cylindrical mass that extends from the posterior ventral aspect of the embryo. The preputial swellings, or external prepuce, are demarcated by a pair of bilateral structures that grow medially to the ventral aspect of the genitalia. In the male embryo, the external prepuce grows around the circumference of the glans and fuses at the ventral midline along the length of the penis (1). Concurrently, the glans and the rest of the penis grows in size. In females, the external prepuce does not completely envelope the genitalia and the glans regresses in size (1). As a result of these developmental differences, the male embryo forms a closed urethra tube situated within the genitalia, which becomes cylindrical and elongated at birth, while in the female, the urethra is not closed, and the genitalia is more oval shaped and shorter than the male. Disruptions in this developmental process could result in atypical genitalia (2).

Congenital defects of the external genitalia are the among most prevalent birth defects, occurring in more than 1:125 births each year (3) and continues to increase in prevalence (4). The mesenchyme of the genitalia is the main organizer of sexually dimorphic developmental events. Both the androgen receptor and estrogen receptor are present in the mesenchyme and transmit male-typic or female-typic signaling pathways (5–7). While the androgen and estrogen receptor are expressed in the epithelium, epithelial-specific knockouts of the androgen and estrogen receptor have no phenotypic differences from normal mice, which suggests no functional role of epithelial steroid receptors in mice (5). Inhibition of androgen signaling in the male embryos with either genetic knockouts or pharmaceutical and toxicological inhibitors results in formation of the clitoris, the female counterpart of the penis (8–10). Thus, the female pathway has been identified as the default/passive developmental pathway because it develops in the absence of androgen signaling. Interestingly, some studies have demonstrated that estrogen signaling prevents outgrowth of penis development (11), and it is hypothesized that it antagonizes androgen signaling in both the male and female external genitalia (5, 12). Indeed, estrogen receptor alpha knockout female mice have longer urethras and are larger in size, while in wild-type male mice, embryonic estrogen exposure reduces penis size and disrupts urethra formation (7). Remarkably, despite the extent to which underlying molecular processes driving genital development have been studied, the etiologies of 70% of genitalia birth defects remain unknown (13, 14).

Here, we used single-cell RNA sequencing during the critical embryonic phase of urethra formation and sexual differentiation to identify cell populations and their lineages in the external genitalia

Significance

Before the onset of sexual differentiation, male and female external genitalia are morphologically indistinguishable. After the onset of sex-specific production of sex steroids by the gonads, the male and female external genitalia differentiate into either a penis or a clitoris. Here, we use single-cell sequencing to investigate the similarities and differences of cell populations in the external genitalia during the critical sexual differentiation window in the mouse embryo. We found that male and female genitalia are largely similar in cell composition and gene expression at the bipotential stage of development. As sexual differentiation ensues, sex steroid–dependent and –independent differences in cell populations arise, leading to dimorphic establishment of the external genitalia.

Author contributions: C.M.A. and H.H.-C.Y. designed research; C.M.A. performed research; C.M.A. analyzed data; and C.M.A. and H.H.-C.Y. wrote the paper.

The authors declare no competing interest.

This article is a PNAS Direct Submission.

[1]To whom correspondence may be addressed. Email: humphrey.yao@nih.gov.

This article contains supporting information online at https://www.pnas.org/lookup/suppl/doi:10.1073/pnas.2103856118/-/DCSupplemental.

Published June 21, 2021.

of mouse embryos, investigate the developmental transcriptomic changes during the sexually dimorphic process, and uncover cell populations (Fig. 1*A*). We first identified the general cell types in the external genitalia of both males and females at three critical developmental stages (Fig. 1*A*). We then focused on the mesenchyme, which play the key role in external genitalia morphogenesis, and further separated the mesenchyme into unique subpopulations with potential genes and pathways that were involved in the developmental changes (Fig. 1*A*). Sexual dimorphism that exists between the subclusters was analyzed for the time-dependent expression of sex steroid–responsive genes. Lastly, we identified unique populations in the male and female genitalia that are likely influenced by different sex steroid signaling.

Results

Characterization of General Cell Populations in the External Genitalia. In the mouse, the bipotential progenitor of the external genitalia is morphologically indistinguishable between male and female embryos at the bipotential stage of development (embryonic day or E14.5; Fig. 1 *B* and *E*). In male embryos, testis-derived androgens transform the progenitor into a penis from E15.5 to E18.5 (15) (Fig. 1 *C* and *D*). On the other hand, in female embryos in which androgens are not produced, the progenitor becomes female biased and eventually develops into the clitoris (15) (Fig. 1 *F* and *G*).

To gain insights into the heterogeneity of the cell populations and their sexual dimorphism, we performed single-cell messenger RNA (mRNA) sequencing using the 10x Genomics 3′ mRNA sequencing platform. Cells were disassociated from male and female external genitalia at three critical time points (E14.5, E16.5, and E18.5) during embryonic development. Each time point includes two separate littermate embryos for each sex, and ∼8,000 cells per replicate were sequenced in a single NovaSeq S2 (Illumina) flow cell at a read depth of ∼40,000 reads/cell. The exact cell numbers and transcript alignment were obtained using Cell Ranger (*SI Appendix*, Table S1).

We first demonstrated that our single-cell sequencing strategy was able to distinguish different cell types for each sex by combining cells from all three development timepoints (Fig. 1 *H* and *I*). Using the R package Seurat V4.0 (16), we identified individual cells by barcodes and clustered them based on similarities of their transcriptomes. Initially we clustered cells with a low resolution (k = 0.02) with the intention to identify the general cell populations that exist in the dataset. To visually present transcriptional and cell population relationships, we used the Uniform Manifold Approximation and Projection (UMAP) dimensionality reduction algorithm (17) to plot and label each cell based on hierarchal clustering. We found that the mesenchyme represented a large proportion of cells in the center, with smaller subpopulations surrounding. To better define these surrounding populations, we increased the clustering resolution to k = 0.3. Including the mesenchyme, we found seven distinct cell populations with clear transcriptional profiles and expression of established cell type–specific markers: mesenchyme [*Col1a1* (18), *Wnt5a* (19), and *Twist1* (20)], endothelium [*Cdh5* (21), *Pecam1* (22), and *Egfl7* (23)], epithelium [*Krt14*, *Krt15*, and *Krt5* (24)], macrophage [*Lyz2* (25), *Cxcl2* (26), and *Il1b* (27)], melanocyte [*Fabp7* (28), *Plp1* (28), and *Ednrb* (29)], smooth muscle [*Acta2* (30), *Itga1* (31), and *Rgs5* (32)], and preputial gland cells [*Cma1* (33), *Cpa3* (34), and *Tpsb2*] (*SI Appendix*, Fig. S1 *A* and *B*). Both male and female external genitalia had the same relative proportion of cell numbers per population and marker genes for each cell population at similar expression levels. This observation indicated that although both male and female external genitalia exhibit strong sexual dimorphisms, they are still composed of the same fundamental cell components.

Dissecting the Mesenchyme of the External Genitalia. Mesenchyme is responsible for developmental changes and tissue remodeling in many organs, including the external genitalia (35–37). By definition, mesenchyme is an undifferentiated, transitive cell population that gives rise to a wide range of connective tissue types and is responsible for key developmental events across the body (38). For example, the mesenchyme that surrounds the open urethra in the penis is largely responsible for the closure of the urethra and formation of a closed tube (39, 40). We therefore focused on the mesenchyme, which represents the largest cell populations in the external genitalia in both sexes (Fig. 1 *H* and *I*). Based on their morphological location, three major mesenchymal cell populations were identified in the external genitalia: corpus cavernosum, glans, and external prepuce (*SI Appendix*, Fig. S2). The corpus cavernosum is situated in the center of the external genitalia as two cylindrical masses that are surrounded by the glans (*SI Appendix*, Fig. S2). The glans is a single cylindrical collection of cells, which are then surrounded by the external prepuce (*SI Appendix*, Fig. S2 *A–C*). The external prepuce circumferentially encloses the glans and fuses along the ventral portion of the genitalia (*SI Appendix*, Fig. S2 *A–C*). Histologically, these three mesenchymal cell populations are distinguishable, although they express distinct markers: SOX9+/NR2F2−/*Hoxa12*− for corpus cavernosum, SOX9−/NR2F2−/*Hoxa12*+ for glanular mesenchyme (*SI Appendix*, Fig. S2 *A–C* and Fig. 2 *D* and *E*), and SOX9−/NR2F2+/*Hoxa12*− for external preputial mesenchyme (*SI Appendix*, Fig. S2 *A–C* and Fig. 2 *I* and *J*) (41, 42).

To further dissect the mesenchymal compartment of the external genitalia, we increased the resolution of the clustering algorithm to k = 0.07. After this unbiased clustering, the cells were revisualized, and marker genes were used to classify each mesenchymal population: *Sox9* for the corpus cavernosum (42) (*SI Appendix*, Fig. S2 *D* and *E*), *Hoxa13* for the glanular mesenchyme (41) (Fig. 2 *A–E*), and an external prepuce marker *Nr2f2* (Fig. 2 *F–J*). We were able to separate these three cell populations based on their transcriptome profiles in both sexes, indicating the validity of our approaches. The corpus cavernosum, glans, and external prepuce mesenchymal populations were verified with other data from https://www.gudmap.org (*SI Appendix*, Fig. S3). We also uncovered markers unique for each population: *Sox5*, *Gpm6b*, *Col9a3*, *Col9a1*, and *Scx* for corpus cavernosum; *Tac1*, *Jag1*, *Hes1*, *Tbx3os1*, and *Col13a1* for the glans; and *Rspo1*, *Fibin*, *Lbh*, *Slc26a7*, and *Akap12* for the external prepuce (*SI Appendix*, Fig. S4 and additional markers listed in Datasets S1 and S2).

Investigation into the Developmental Program in the Glanular Mesenchyme. Further interrogation of single-cell data revealed heterogeneity within the glanular and preputial mesenchyme, while the corpus cavernosum was a homogenous cell population. We then separated the glanular (*Hoxa13*+) and preputial (*Nr2f2*+) cell populations and reclustered them, see Figs. 3 and 4. Glanular and preputial mesenchyme both play essential roles in the development of the external genitalia. Both populations directly undergo significant morphological changes during sexual differentiation and play essential functional roles in adulthood. We first investigated the diversity of the glanular mesenchyme by increasing the clustering stringency to k = 0.12 (Fig. 3 *A–C*). With this clustering, we identified three mesenchymal populations in the glans of both the male and female: distal dorsal, distal ventral, and proximal glanular mesenchyme (Fig. 3 *A–C*). In both sexes, unique markers were found to demarcate the distal dorsal (*Inhba*, *Alx4*, *Syt13*, and *Dkk1*), distal ventral (*Dlx5*, *Scube1*, *Notum*, *Hand2*, and *Ahr*), and proximal glans (*Gli1*, *Foxl2*, *Foxf2*, and *Foxd1*) (Fig. 3 *D* and *E* and *SI Appendix*, Fig. S5*A* and Datasets S3 and S4). In the male, both proximal and distal ventral glans had time-dependent clusters, signifying the occurrence of a large amount of transcriptional changes. In the female, we only detected a time-dependent reclustering of the proximal mesenchyme but not the distal ventral mesenchyme (Fig. 3 *A* and *C*). The proximal mesenchyme in the female underwent a larger expansion, starting with 1,017 cells at the bipotential stage and expanding to 6,182 cells at the late differentiation

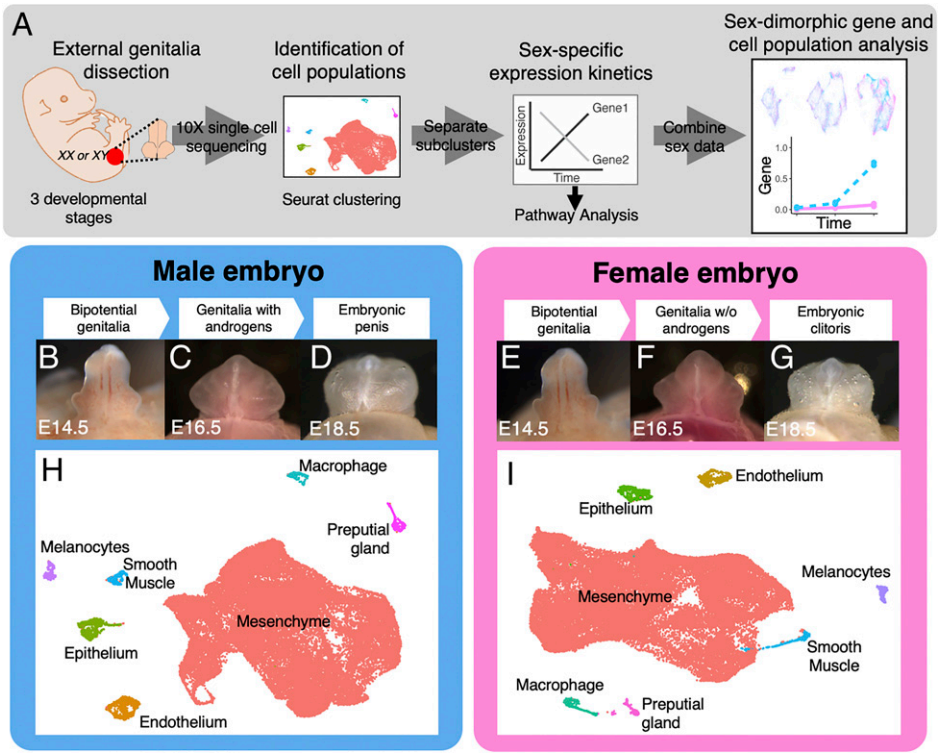

Fig. 1. Single-cell sequencing analysis of mouse external genitalia. (*A*) Workflow of single-cell sequencing analysis. (*B–G*) Whole mount images of male and female external genitalia of mouse embryos at three developmental stages for single-cell sequencing. (*H* and *I*) UMAPs of the general cell clusters of male and female samples that are based on all cells from the three developmental stages combined. Each dot represents a single cell, and the color of the cell is the population it belongs to. (*J* and *K*) Dot plots of marker genes that are enriched in different cell populations in the male and female genitalia from *H* and *I*, respectively. The dot size represents the percentage of cells that express the gene and, the color represents the intensity of expression (red = high and blue = low).

stage. The male started with 850 cells and had 2,885 cells by late differentiation, making the relative increase in cells over two times higher in the female. Using fluorescent RNA in situ hybridization to detect mRNA expression of three markers specific to each subpopulation (*Inhba* for distal dorsal, *Dlx5* for distal ventral, and *Gli1* for proximal glanular mesenchyme in Fig. 3 *F* and *G*), we confirmed the region-specific expression patterns of these genes and identified unique patterns within each domain. The distal mesenchyme is closer to the tip of the external genitalia and has less interaction with the external prepuce (Fig. 3*B*), while the proximal mesenchyme is closer to the base of the external genitalia, and there are extensive interactions with the external prepuce. Our data revealed a clear delineation where the prepuce-enveloped glans is positive for *Gli1* but negative for *Inhba* and *Dlx5*. Where the external prepuce ends, *Gli1* expression is turned off, and *Inhba* and *Dlx5* expression starts. We also confirmed that at late sex differentiation (E18.5), the proximal cell population was positive for *Mfap5* in both male and female, and this cell type largely surrounds the urethra (*SI Appendix*, Fig. S5*B*).

After successfully identifying the cell populations in the glans, we focused on investigating the progression of each cell population through the different developmental stages with the identification of the genes that were associated with the sex-specific and cell population–specific shifts over time. All the mesenchymal populations in the glans had time-dependent shifts in transcriptomes regardless of the sex. In the male, these shifts from E14.5 to E18.5 were characterized by expression of *Myl12a*, *Myl6a*, *Greb1*, and *Notum* in the distal ventral mesenchyme; *Lamc3*, *Coch*, *Inhba*, and *Notch2* in the distal dorsal mesenchyme; and *Lgr5*, *Des*, *Mafb*, and *Slain1* in the proximal mesenchyme (Fig. 3*H* and *SI Appendix*, Fig. S5, *Des* UMAP through time). In the female, these shifts were characterized by expression of *Esr1*, *Efna5*, *Igfbp5*, and *Igfbp2* in the distal ventral mesenchyme; *Bmp4*, *Bmpr2*, *Gap43*, and *Fabp5* in the distal dorsal mesenchyme; and *Stc1*, *Col15a1*, *Aldh2*, and *Sep15* in the proximal mesenchyme (Fig. 3*I*). Pseudotime analysis for the distal ventral and proximal glans was conducted, and similar relationships were found for each of the genes (*SI Appendix*, Fig. S6).

To identify the biological context of cell type–specific and sex-biased gene changes in the glans, we then performed Ingenuity Pathway Analysis (IPA) on the genes differentially regulated in three glanular mesenchymal subpopulations (Fig. 3 *J–L*). In the distal ventral mesenchyme, the "coronavirus pathway" was up-regulated in the female (Fig. 3*J*). The coronavirus pathway incorporates processes of endocytosis, transcription, and protein packaging. This suggests that the females are receiving paracrine signals and transcribing them into gene expression changes. The male genitalia had up-regulation of the "apelin endothelial pathway" and "actin cytoskeleton signaling pathway" (Fig. 3*J*). These pathways represent the extension of blood vessels to the tip of the penis and changes of cell morphology to facilitate urethra closure in the male. In the distal dorsal mesenchyme, there was a down-regulation of "PTEN signaling" and an up-regulation of "NF-kB" and "BMP signaling" in the female, while the male had very few differentially regulated pathways (Fig. 3*K*). BMP signaling is associated with phallus size reduction (43), and both BMP and NF-κB suppress PTEN signaling (44, 45). PTEN signaling modulates cell proliferation and apoptosis, which may be involved in controlling the size of the female genitalia (46). In the proximal mesenchyme, there was an up-regulation of "Wnt signaling" and "Ahr signaling" and down-regulation of "EMT in development pathway" in the male, while the female had few differentially regulated pathways (Fig. 3*L*). Wnt and EMT are both involved in penis development and facilitate urethra closure (47, 48). Ahr is an environmental-sensing nuclear receptor that influences the immune system and response to

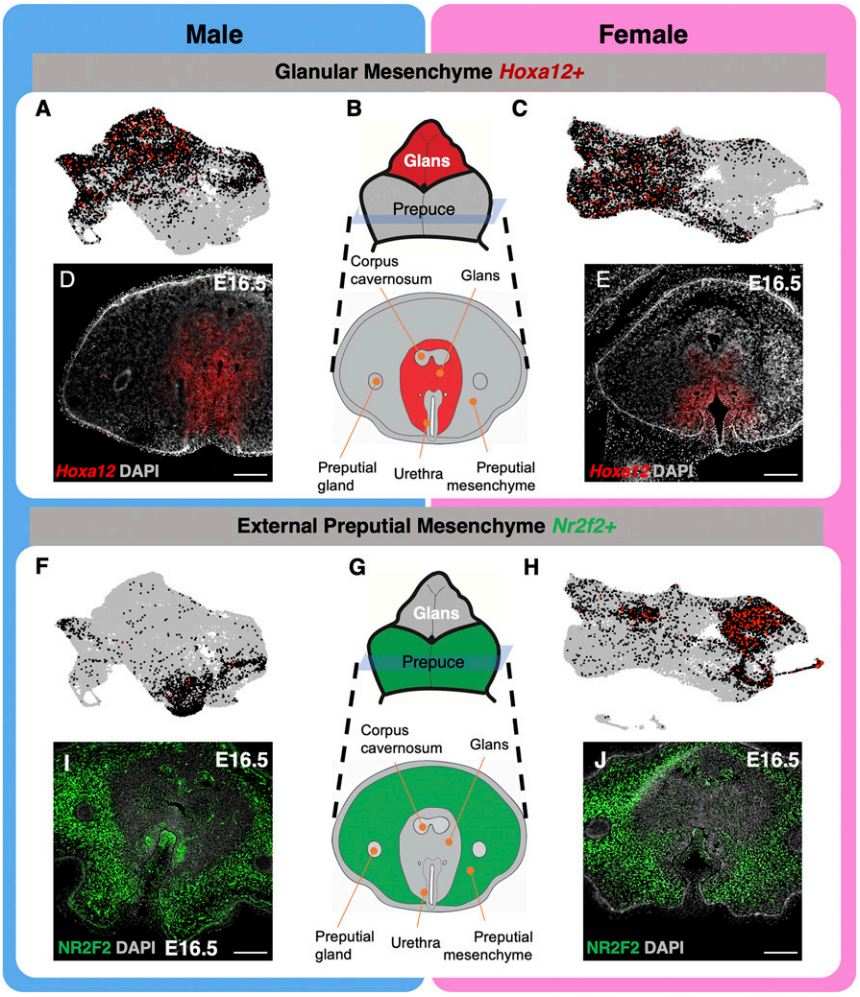

Fig. 2. Characterization of mesenchymal cell populations identified in single-cell sequencing. (*A* and *C*) UMAPs of glanular mesenchyme cell clusters that are positive for *Hoxa12* (black and red dots) in male and female external genitalia. Each gray dot represents a cell with no expression of the gene, each black dot represents a cell with modest expression, and each red dot represents a cell with high gene expression. (*B*) Whole mount and cross-section representation of external genitalia that highlight the glans and glanular mesenchyme in red. (*D* and *E*) In situ hybridization of *Hoxa12* (red) and DAPI counterstain (gray) on cross-sections of male and female genitalia. (*F* and *H*) UMAPs of preputial mesenchyme clusters that are positive for *Nr2f2* (black and red dots) in male and female external genitalia. (*G*) Whole mount and cross-section representation of the external genitalia that highlight the external prepuce and preputial mesenchyme in green. (*I* and *J*) Immunofluorescence of NR2F2 (green) and DAPI counterstain (gray) in the external genitalia of the male and female genitalia. (Scale bars, 100 μm.)

exogenous toxicants (49). Single-nucleotide polymorphisms in *Ahr* are associated with hypospadias in humans (50).

Investigation of the Developmental Program in the External Prepuce. We next investigated the diversity of the preputial mesenchyme by increasing the clustering resolution to k = 0.12 (Fig. 4 *A*–*C*) on the *Nr2f2* cell population. We found two external prepuce populations in both sexes: general prepuce and subdermal prepuce (Fig. 4 *A* and *C*). The general prepuce population in the male can be further separated into three subclusters according to the developmental stages (Fig. 4*A*). Although these three subclusters exhibited stage-specific transcriptomes, they all expressed general prepuce-specific genes including *Akap12*, *Pde3a*, *Tfap2a*, and others (Fig. 4*D* and *SI Appendix*, Fig. S7*C* and Datasets S7 and S8). *Akap12* does not mark the entirety of the external prepuce but rather a certain proportion of the general prepuce. The subdermal prepuce population in the male, on the other hand, did not show any stage-specific difference and was marked by distinct lineage markers (*Irx1*, *Penk*, and *Icam1*) (Fig. 4 *A* and *D*). We did find *Irx1* to be present in the bipotential general prepuce (E14.5), but there was not enough enrichment of other genes in this subgroup to define it as a unique population. *Irx1* may be a progenitor marker for the subdermal prepuce. In the female, the general prepuce followed a stage-specific pattern similar to the male with the separation of three subclusters based on developmental stages (Fig. 4 *C* and *E*). The *Irx1*-postive subdermal prepuce did not separate into time-dependent subpopulations (Fig. 4*C*). Using immunofluorescence to detect protein expression of markers specific to each subpopulation (AKAP12 for general prepuce and IRX1 for subdermal prepuce Fig. 4 *F* and *G*), we confirmed the region-specific expression patterns of these genes and identified unique patterns within each domain.

After investigating the cell populations in the external prepuce, we explored the genes that were associated with the sex-specific and cell population–specific transcriptomic shifts. In the male, the shifts in the subdermal prepuce were characterized by *Nfe2l2*, *Grem1*, *Foxf2*, and *Gadd45gip1*, and the general prepuce transcriptomes were characterized by expression of *Myl9*, *Gdf10*, *Sox4*, and *Igf1* (Fig. 4*H*). In the female, the subdermal prepuce shifts were characterized by expression of *Fgfr2*, *Notch1*, *Akr1b3*, and *Msmo1* and the general prepuce by *Tgfb2*, *Enpp2*, *Gpx8*, and *Mylk* (Fig. 4*I*).

To identify the biological context of cell type–specific and sex-biased gene changes in the glans, we then conducted IPA on the genes differentially regulated in subdermal mesenchyme and general prepuce in the male and female genitalia (Fig. 4 *J* and *K*). In the subdermal prepuce, we found the "Nrf2-related pathway" down-regulated and the "GP6 signaling pathway" up-regulated in male, while the "Il-15 signaling pathway" was up-regulated in the female (Fig. 4*J*). *Nrf2* is an environmental-sensing transcription factor that is involved in the expression of phase I and phase II detoxification enzymes (51). Glycoprotein IV (GP6) is largely involved in the sensing of the extracellular environment. GP6 is both a receptor for collagen, laminin, and fibrin and a regulator of *Adams* and *Adamnts* gene expression (52). Interleukin 15 (Il-15) is secreted by muscle cells to promote further myogenesis (53). In

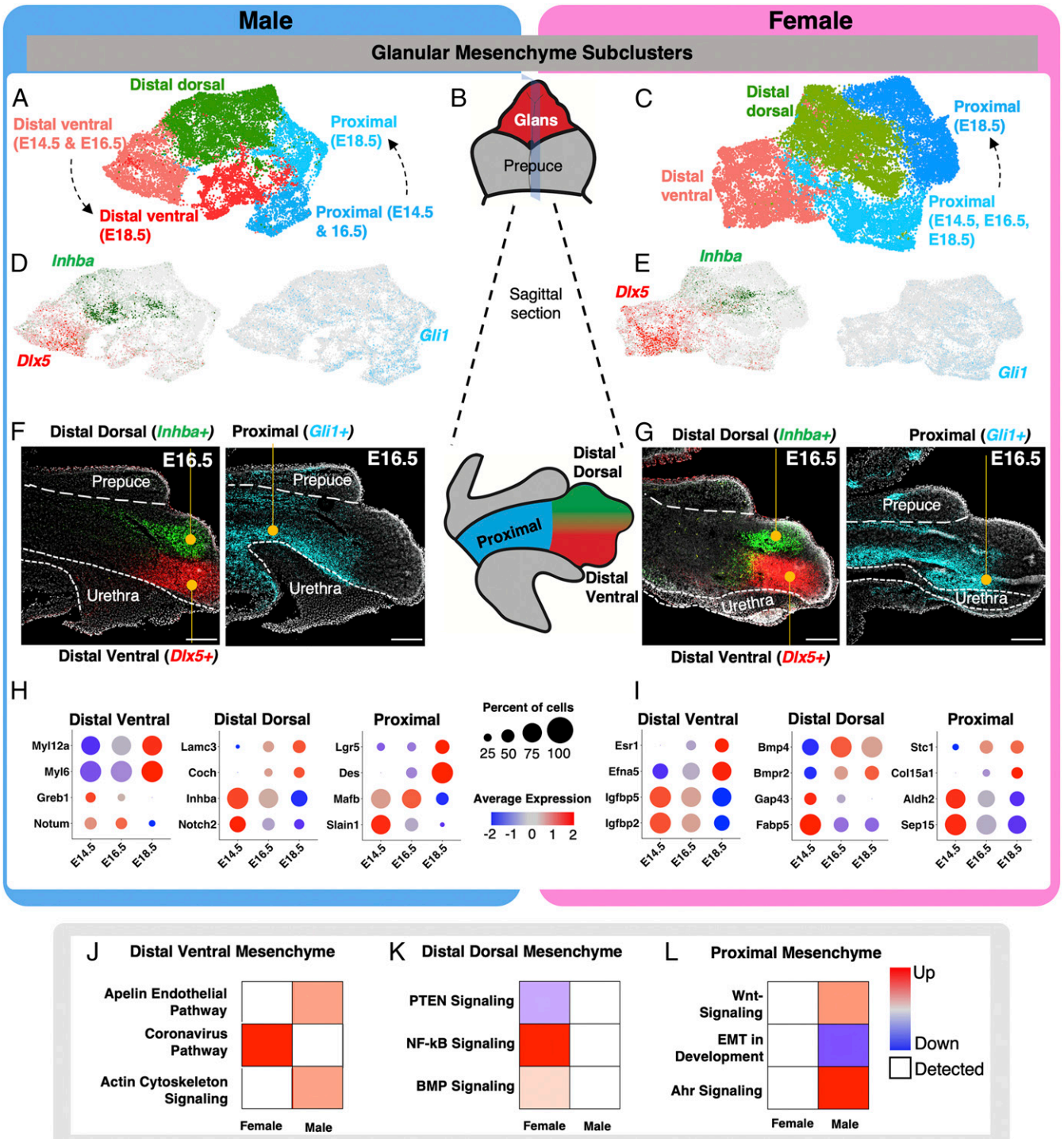

Fig. 3. Identification of unique subpopulations in the glanular mesenchyme. (*A* and *C*) Reclustering of the glanular mesenchymal cells in male and female from Fig. 2 with higher resolution. The different colored cells represent distinct cell clusters identified with unbiased clustering. (*B*) Whole mount and sagittal-section representation of external genitalia that highlight the glans in red (whole mount), external prepuce in gray (whole mount), proximal glans in blue (sagittal), distal dorsal glans in green (sagittal), and distal ventral glans in red (sagittal). (*D* and *E*) UMAPs of glanular mesenchyme subclusters in *A* and *C*, respectively, that are positive for *Inhba* (green), *Dlx5* (red), and *Gli1* (light blue). (*F* and *G*) In situ hybridization for *Inhba* (green), *Dlx5* (red), and *Gli1* (light blue) on sagittal sections of external genitalia. The external prepuce and urethra portions of the external genitalia are outlined with dotted lines and with the glans in the center. (*H* and *I*) Dot plots of marker genes that are enriched in different cell populations in the male and female genitalia from *A* and *C*, respectively. The dot size represents the percentage of cells that express the gene, and the color represents the intensity of expression (red = high and blue = low). (*J*–*L*) Pathway analysis of genes that were identified in *H* and *I*. The pathways were selected based on whether they were unique to male or female development. Red = up-regulated, blue = down-regulation, white = detected, and circle size = *P* value of the pathway. (Scale bars, 100 μm.)

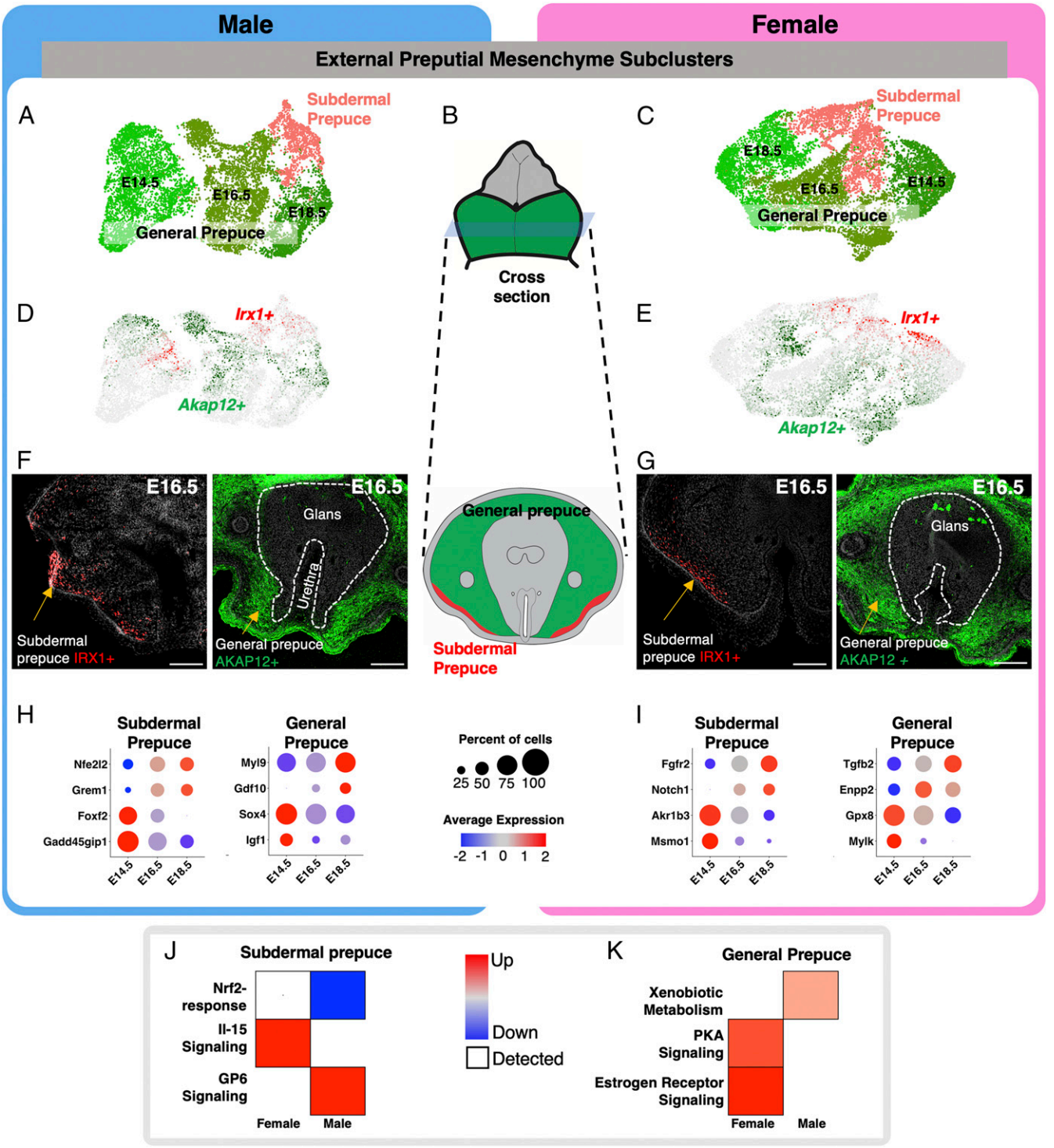

Fig. 4. Identification of unique subpopulations in the external preputial mesenchyme. (*A* and *C*) Reclustering of the preputial mesenchymal cells in male and female from Fig. 2 with higher stringency. The different colored cells represent distinct cell clusters identified with unbiased clustering. (*B*) Whole mount and cross-section representation of external genitalia that highlight the external prepuce in green and glans in gray. (*D* and *E*) UMAPs of preputial mesenchyme subclusters in *A* and *C*, respectively, that are positive for *Akap12* (green) and *Irx1* (red). (*F* and *G*) Immunofluoresence for IRX1 (red) and AKAP12 (green) on cross-sections of external genitalia. The external prepuce and urethra portions of the external genitalia are outline with dotted lines and with the glans in the center. (*H* and *I*) Dot plots of marker genes that are enriched in different cell populations in the male and female genitalia from *A* and *C*, respectively. The dot size represents the percentage of cells that express the gene, and the color represents the intensity of expression (red = high and blue = low). (*J* and *K*) Pathway analysis of genes that were identified in *H* and *I*. The pathways were selected based on whether they were unique to male or female development. Red = up-regulated, blue = down-regulation, and circle size = significance of the pathway. (Scale bars, 100 μm.)

https://doi.org/10.1073/pnas.2103856118

the general prepuce, we found the "xenobiotic metabolism" pathway up-regulated in the male, while "estrogen receptor signaling" and "protein kinase A signaling" were up-regulated in the female (Fig. 4*K*). The xenobiotic metabolism pathway involves the up-regulation of phase I and II detoxification to help combat exogenous targets that disrupt normal biological processes (54). Estrogen receptor signaling is composed of estrogen-responsive genes and coregulators of estrogen receptor. The protein kinase A pathway has a broad array of function. Specifically, in mesenchymal tissue and muscle, proteins kinase A interacts with AKAP proteins to facilitate muscle function (55).

Hormone-Dependent Sexual Dimorphisms in the External Genitalia. It is well established that androgens are essential for penis development (56). To a lesser extent, estrogen is beginning to be recognized for its role in clitoral differentiation (56). To use single-cell sequencing to gain insights into how these sex steroids act in the external genitalia, we combined the male and female datasets with all three developmental stages and identified sexually dimorphic clusters and genes related to specific hormone-responsive pathways. We first observed that glanular and preputial mesenchyme were separated with their distinct subpopulations (proximal versus dorsal distal versus ventral distal in the glans and general versus subdermal in the external prepuce) in a stage-specific manner (E14.5, E16.5, and E18.5), further confirming the validity of our analytic strategies (Fig. 5 *A* and *B* and *SI Appendix*, Fig. S8*A*). The second observation was that the cell clustering in the glans at the bipotential (E14.5) and early differentiation stages (E16.5) was nearly identical between male and female in the dorsal distal, proximal, and ventral distal regions, with only zero, six (four male up-regulated and two female up-regulated), and one (one female up-regulated) differently regulated genes at E14.5 and nine (seven male up-regulated and two female up-regulated), 29 (16 male up-regulated and 13 female up-regulated), and five genes (five male up-regulated) at E16.5 (Fig. 5*A*). However, at the late genitalia differentiation stage (E18.5), male and female cells in the glans became separated in each region with 203 (87 male up-regulated and 116 female up-regulated, dorsal distal region), 253 (128 male up-regulated and 125 female up-regulated, proximal region), and 229 (109 male up-regulated and 120 female up-regulated, ventral distal region) displayed a trend similar to that in the glans. At the bipotential stage (E14.5), the general prepuce was nearly identical between male and female with three (three up-regulated male) differentially regulated genes (Fig. 5*B*). By early sexual differentiation (E16.5), the external prepuce divided into two subpopulations, subdermal and general prepuce. In the subdermal prepuce, there were 71 (48 male up-regulated and 23 female up-regulated) genes, and in the general prepuce, there were 25 (7 male up-regulated and 18 female up-regulated) genes. At E18.5 or the point of genitalia differentiation, the male and female preputial mesenchyme became more distinctly separate from each other, and 124 (63 male up-regulated and 61 female up-regulated) in the subdermal prepuce and 184 (109 male up-regulated and 75 female up-regulated) in the general prepuce were differently regulated between male and female (Fig. 5*B*).

We next investigated whether the mesenchyme of glans and external prepuce respond to androgen and estrogen differently by examining the expression of steroid-responsive genes. First, we investigated genes related to the androgen signaling pathway, which is known to control normal male penis development (57) (Fig. 5*C*). Androgens bind the androgen receptor (*Ar*), which then drives male-typic gene expression (58). *Ar* was abundantly expressed in up to 73% of external genitalia cells in both the male and female external genitalia (*SI Appendix*, Fig. S8*B*). Each subpopulation of the mesenchyme in the genitalia expressed *Ar* (Fig. 5*C*). At the bipotential (E14.5) and early differentiation (E16.5) stages, there were no sexual dimorphisms in *Ar* expression across all tissues and subpopulations (Fig. 5*C*). In contrast, at E18.5, female genitalia had significantly higher levels of *Ar* mRNA in all but the general prepuce subpopulations (Fig. 5*C*). We also investigated the expression of 5α-reductase type II (*Srd5a2*), the enzyme that converts testosterone to the more potent androgen dihydrotestosterone (*SI Appendix*, Fig. S8*C*). We found both male and female had low *Srd5a2* expression in all tissues at bipotential and early differentiation stages (*SI Appendix*, Fig. S8*C*). By late differentiation, all tissues up-regulated *Srd5a2*, and the only tissue with significant sexual dimorphism was the ventral glans mesenchyme (*SI Appendix*, Fig. S8).

Next, we examined the androgen responsiveness of each tissue and subpopulations. Metallothionein 1 (*Mt1*) is an androgen-responsive gene in a number of androgen-responsive tissues including the embryonic genitalia (59, 60). Within the glans, the proximal, distal dorsal, and distal ventral populations had similar expression dynamics of *Mt1* (Fig. 5*C*): little to no expression in both sexes at the bipotential stage (E14.5) and early differentiation (E16.5) and a significant up-regulation at the late differentiation stage (E18.5) only in the male. In the external prepuce, *Mt1* expression dynamics exhibited sexually dimorphic patterns with a significant increase in the male at E16.5 and E18.5 (Fig. 5*C*).

Smooth muscle actin (*Acta2*) is another androgen-responsive gene that is responsible for smooth muscle differentiation in genitalia and other urogenital structures (61). In all three glans subpopulations, there was little *Acta2* gene expression and no time- or sex-dependent differences in gene expression. In the external prepuce, the subdermal prepuce had little expression of *Acta2* at the early bipotential stage. From the early and into the late differentiation stages, a significant increase in *Acta2* was found in male but not in the female. The general prepuce followed a similar trajectory with the exception that *Acta2* expression at E18.5 was double the expression in the subdermal prepuce (Fig. 5*C*).

We next investigated estrogen receptor and estrogen-responsive genes and their differential expression across genitalia cell populations. Estrogen receptor alpha (*Esr1*) was only expressed in up to 6% of cells in the external genitalia (*SI Appendix*, Fig. S8*B*). Estrogen receptor beta or *Esr2* had little to no expression throughout the genitalia with a nonsignificant enrichment in the ventral glanular mesenchyme (*SI Appendix*, Fig. S8*C*). Expression of the G-coupled estrogen receptor (*Gper1*) was low with a modest, nonsignificant enrichment in the subdermal prepuce. We also investigated the enzyme that converts testosterone to estrogen (*Cyp19a1*) and found little to no expression in all tissues (*SI Appendix*, Fig. S8*C*). Unlike *Ar*, *Esr1* has more unique expression within the glanular and preputial mesenchyme (*SI Appendix*, Fig. S8*C*). In the glans, both the proximal and ventral glans populations had similar dynamics of *Esr1* expression, with the distal ventral mesenchyme starting with a higher baseline expression (Fig. 5*C*). Both populations exhibited small increases from E14.5 to E16.5. By E18.5, the female had a significant increase in *Esr1* expression, while the male expression did not change (Fig. 5*D*). The distal dorsal subpopulation, however, had little to no *Esr1* expression throughout the developmental series.

Collagen type 15 alpha 1 chain (*Col15a1*) is a type of collagen found in skeletal muscle and potentially inhibits angiogenesis (62). Ethinyl estradiol exposure increases *Col15a1* expression in uterine tissue (63, 64). In the glans subpopulations, the distal dorsal and distal ventral both showed time-dependent increases of *Col15a1* expression. There was a slight up-regulation in the male at E18.5 in the distal ventral mesenchyme. In the proximal glans, both male and female had similar expression at the bipotential stage. Similar patterns were found at E16.5, but by E18.5, the female had significantly higher expression of *Col15a1* than the male (Fig. 5*D*). In the external prepuce, the general prepuce had similar expression between the sexes at the bipotential stage. At E16.5, there was a slight sexual dimorphism in which the female

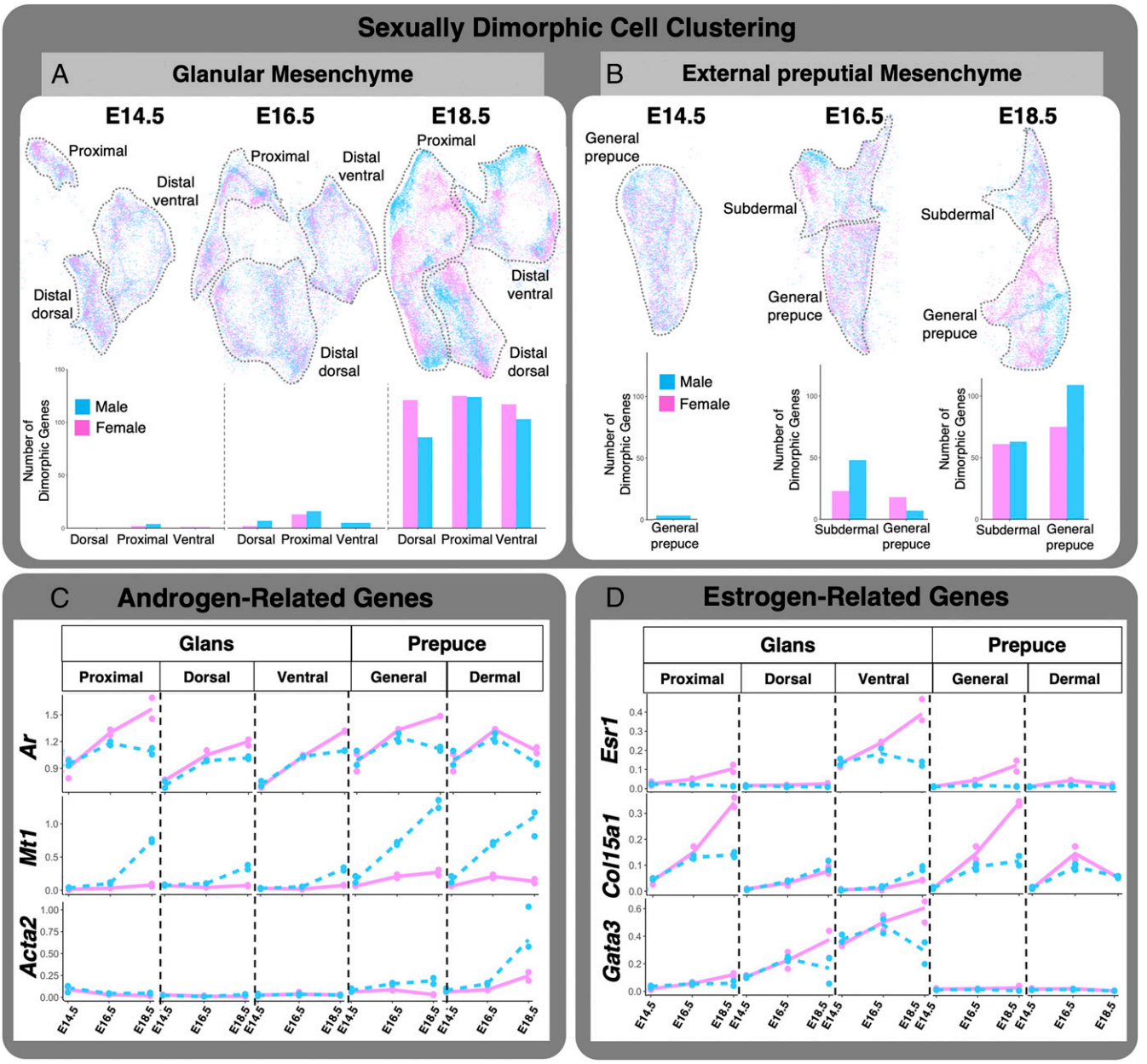

Fig. 5. Sexual dimorphic expression of androgen- and estrogen-related genes. (*A*) Glanular and (*B*) preputial mesenchyme UMAP of both male (blue) and female (pink) data combined. The bar graphs represent sexually dimorphic gene expression identified in each of the cell populations for each developmental time point. (*C* and *D*) Transcriptional kinetics of androgen- and estrogen-related genes in each of the identified subpopulations (blue = male and pink = female).

had higher expression, but by E18.5, the difference disappeared. In the subdermal prepuce mesenchyme, both the male and female had little to no expression of *Col15a1*. By E16.5, there was slightly higher expression in the female, and by E18.5, the female had three times the expression of *Col15a1* than that of the male.

GATA binding protein 3 (*Gata3*) establishes a positive feedback loop with *Esr1* in several tissues that are involved in the differentiation of estrogen-dependent cell lineages (65). In the glans, the subpopulations displayed similar expression patterns, but each population started at a different baseline (Fig. 5*D*). The proximal glans had the lowest expression, distal dorsal was in between, and distal ventral had the highest expression of *Gata3*. At the bipotential stage, *Gata3* expression was the same across the glans cell populations and sexes (Fig. 5*D*). By the stage of full embryonic genitalia differentiation, *Gata3* was significantly increased in the female genitalia but not the male (Fig. 5*D*). The distal ventral glans was the only population that was significantly sexually dimorphic at E18.5. The external prepuce population had very little *Gata3* expression and no sex- or time-dependent difference of gene expression (Fig. 5*D*).

Identification of Sexually Dimorphic Cell Populations in the External Genitalia. A powerful aspect of single sequencing and unbiased statistical clustering is the identification of new and rare cell populations. We increased the clustering resolution to k = 0.3 and searched for mesenchymal populations that are present in one sex but absent (or in very low abundance) in the other sex. First, we investigated the glanular mesenchyme and identified 11 cell populations in the male and only 10 in the female (Fig. 6 *A* and *B*).

The population unique to the male was found in the broader proximal and distal ventral glanular mesenchyme and marked by expression of androgen-responsive genes including *Mt1* (Fig. 6*C* versus Fig. 6*D*), *Mt2*, *Fst*, and others (*SI Appendix*, Fig. S9). In the external prepuce mesenchyme, nine cell populations were identified in the male, whereas 10 were found in the female genitalia (Fig. 6*E* versus Fig. 6*F*). The unique female-specific cell population was incorporated within the general prepuce mesenchyme and enriched with *Esr1* (Fig. 6*G* versus Fig. 6*H*), *Cxcl12*, *Col15a1*, and other estrogen-responsive genes (*SI Appendix*, Fig. S9). Those genes had much lower expression in surrounding populations of the male external prepuce (Fig. 6*G*).

Discussion

Insights into Morphogenesis of the External Genitalia. The development of the external genitalia is a highly orchestrated process in which multiple cell populations are involved in shaping and making a functional organ. We used single-cell sequencing to unbiasedly classify the three major tissues of the external genitalia, the corpus cavernosum, glans, and external prepuce. Expectedly, at the bipotential stage of development, the corpus cavernosum, glans, and external prepuce have already separated into three distinct cell populations (Fig. 7). The corpus cavernosum, a structure that runs the length of the dorsal aspect of the glans, functions as the erectile tissue of the genitalia that aids in copulation. In our single-cell data, the corpus cavernosum was a homogenous population that underwent little morphological and transcriptional changes throughout development. On the other hand, the glans and the external prepuce were both heterogenous and underwent significant morphological and transcriptional changes through development (Fig. 7). After unbiased clustering, the glans separated into the distal dorsal, distal ventral, and proximal cell populations, and the external prepuce separated into the general and subdermal cell populations of the external prepuce.

The glans is the copulatory organ in the adult male that houses the urethra in the center of the structure (66). In the female, in contrast, the urethra is not internalized and remains open along the ventral aspect of the genitalia throughout embryonic development. The urethra of the female mouse will eventually be tubularized through undetermined mechanisms and exit near the tip of the clitoral structure postnatally (67). The sexually dimorphic closure of the urethra is initiated at the bipotential stage of development (E14.5 in the mouse). In the male embryo, urethra closure occurs in a proximal-to-distal wave, where two lateral portions of the ventral and proximal glanular mesenchyme undergo a medial fusion and make a urethral tube. This process eventually reaches the distal aspect of the penis and does not occur in the female (68). Our single-cell data revealed that at the bipotential stage, the male and female have similar cell population profiles in the proximal and distal ventral aspects of the glanular mesenchyme, which directly contact the urethra. However, the proximal and distal ventral mesenchyme are different transcriptionally in both sexes: by late sexual differentiation when the penis is forming, the proximal and distal ventral mesenchymal populations become transcriptionally similar in the male with the enrichment of smooth muscle-related genes, which is consistent with the smooth muscle structures that surround the urethra and support urination and ejaculation (69). In the female, on the contrary, the distal ventral mesenchyme becomes even more distinct from the proximal mesenchyme. We argue that because urethra closure does not happen in the female embryo, proximal mesenchyme and distal ventral populations do not need to initiate similar transcriptomes to propagate production of a tube and instead continue on their own differentiation trajectory (Fig. 7).

The external prepuce, which is present in both sexes (70), completely envelops the glans in the male but remains unfused in the female, except at the proximal portion of the genitalia. The unfused external prepuce in the female reveals the open urethra and the ventral glans of the female genitalia. Cell populations in the external prepuce exhibited similar transcriptional changes in both sexes during development, and no differences in the composition of external prepuce subpopulations were found between the sexes. The external prepuce largely consisted of a general prepuce with a smaller subdermal population along the outer edge of the external prepuce, which is only observed until now with the resolution of single-cell sequencing. Based on the expression of cell-adhesion marker *Icam1* (71) and prostate stromal cell marker *Penk* (72), we suspect this cell population eventually differentiates into a muscle layer of the external prepuce similar to the dartos fascia in humans (73).

Dissecting the Morphogenetic Pathways in Genitalia Differentiation. BMP and WNT are two classical developmental pathways involved in external genitalia development (41, 47). Although these pathways have been studied extensively, how they interact among different cell populations in a sexually dimorphic manner remains to be clearly defined. BMP signaling induces apoptosis, reduces cell proliferation, and inhibits overall outgrowth of the mouse genitalia (43, 74). We discovered that BMP ligand *Bmp4* and receptor *Bmpr2* are produced by the majority of the cells in the external genitalia in both sexes; however, these two ligands are specifically up-regulated in the mesenchymal cell population only in female dorsal glans (Fig. 7). This means there is both a sexual dimorphic regulation of the BMP pathway and response to BMP signaling in the external genitalia. It is known that activation of the WNT signaling pathway is tightly linked to the development of the male external genitalia (47). WNT receptors *Fzdb* and *Fzd1*-6 and downstream transcription factors *Lef1* and *Tcf7l1* are elevated in the male external genitalia, whereas WNT inhibitors *Dkk2* and *Sfrp2* are up-regulated in the female (57). Using real-time PCR on microdissected external genitalia, Miyagawa et al. (47) were unable to detect the expression of WNT ligands *Rspo1*, *Rspo2*, and *Rspo3* in the male and female genital tubercle at E15.5. We found expression of both *Rspo1* and *Rspo3* in the external prepuce and in the distal aspect of the ventral glans throughout sexual differentiation. The coreceptor for the WNT ligand *Rspo1* receptor, *Lgr5*, was expressed in the proximal glans in both male and female genitalia. WNT inhibitors *Notum*, located in the distal ventral mesenchyme, and *Gadd45gip1*, located in the subdermal prepuce, were down-regulated in a male-specific manner (Fig. 7). The prominence of WNT-related genes in the ventral glans, proximal glans, and external prepuce suggests they interact with already known WNT molecules, are involved in urethra closure, and are important for the sexually dimorphic development of the external genitalia.

In addition to these pathways known for external genitalia development, our single-cell analyses uncovered players in this process. We found that inhibin beta A subunit (*Inhba*) had a very specific expression domain in the distal dorsal aspect of both the male and female genitalia. *Inhba* encodes the subunit for activins and inhibins, secreted factors in the TGF-B superfamily that are involved in the development and function of several mesenchymal-derived cells (75). *Inhba* can homodimerize to form activin A or can heterodimerize with inhibin beta B subunit (*Inhbb*) to form activin AB (76); both are ligands that can induce biological functions. One study reported that the replacement of *Inhba* with *Inhbb* caused an enlargement of the clitoris and penis (75), which is independent of the action of testosterone or dihydrotestosterone. In addition to the activin ligand, we found that follistatin, a strong antagonist of activin, is enriched in the distal ventral and proximal aspects of the glans of the male external genitalia. We speculate that follistatin may antagonize the action of activin from the distal dorsal mesenchyme to promote male genitalia outgrowth. Concurrent with the elevated *Fst* expression, the male had a significant decrease of *Inhba* expression in the distal dorsal mesenchyme, while the female maintained expression of *Inhba*,

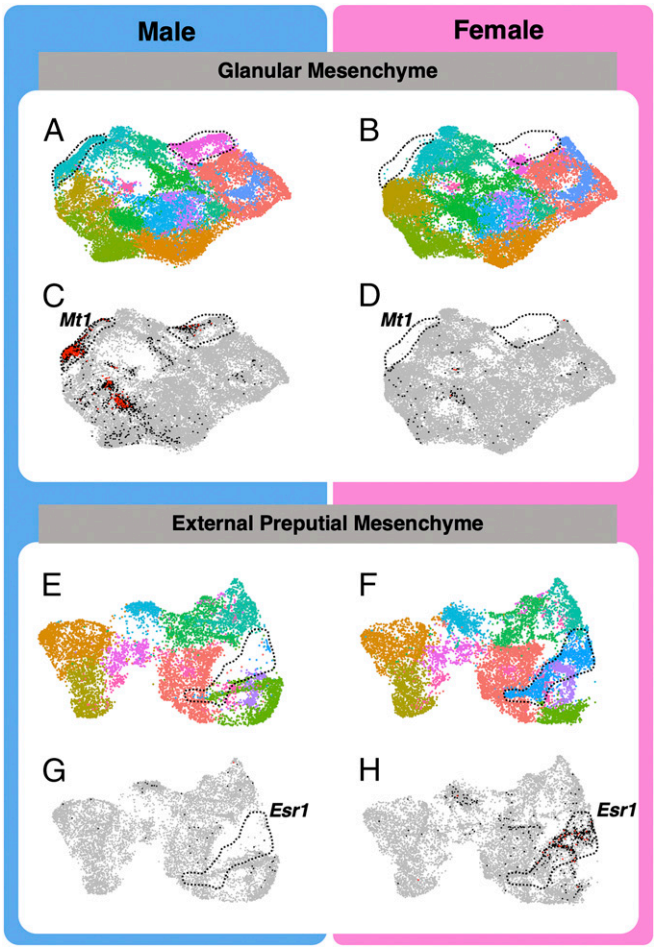

Fig. 6. Identification of cell populations in the glanular and preputial mesenchyme with specific responsiveness to androgen and estrogen. (*A*, *B*, *E*, and *F*) Higher-resolution clustering of the two glanular and preputial mesenchyme to identify cell types. The color represents different cell clusters, and the dotted lines display the presence of a cluster in the male and the absence in the female glanular mesenchyme. (*C* and *D*) Sex-specific cell cluster enriched with androgen-sensitive marker gene (*Mt1*), and (*G* and *H*) cell cluster enriched with estrogen receptor 1 (*Esr1*). Each gray dot represents a cell with no expression of the gene, each black dot represents a cell with modest expression, and each red dot represents a cell with high gene expression.

implicating a potential role of the activin/follistatin pathway in external genitalia fate.

Mapping the Action of Androgen and Estrogen in External Genitalia. Sexually dimorphic formation of the external genitalia requires proper action of sex steroid androgens and estrogens. In the event of compromised sex steroid action, congenital defects of the external genitalia arise. Androgen and estrogen signaling pathways are involved in normal external genitalia formation (77). Proper genitalia formation requires a tight coordination of all neighboring cells (78). Our single-cell sequencing results indicate a strong sexual dimorphism of *Ar* and *Esr1* expression in the proximal glans and general prepuce and a strong sexual dimorphism of *Esr1* in the ventral glans mesenchyme. As expected, each of these cell populations express genes induced by these two hormones. However, the expression kinetics of these steroid-responsive genes exhibit tissue specificity, suggesting regulatory mechanisms other than traditional transcriptional regulation in each of the cell populations. We propose that each cell population develops in synchrony due to the presence of sex steroids, while differential responses to hormones allow each population to play a unique role in development. Based on our data, we hypothesize that sex steroid signaling resulted in large transcriptomic differences in the distal ventral and general prepuce and are directly associated with sites of morphological sexual dimorphism and potential areas of congenital defects.

Although steroids play a major role in sexual differentiation, there are steroid hormone-independent developmental processes in the external genitalia (79). The dorsal mesenchyme had little *Esr1* expression, no sexual dimorphism of *Ar* expression, and little to no sexual dimorphism in a number of key sex steroid–responsive genes. Although there is not much evidence of steroid signaling in the dorsal mesenchyme, there are still strong sexual dimorphisms that exist. The dorsal mesenchyme had more female genes upregulated than the male and had more differentially regulated biologic pathways in the female, indicating a divergence in the sexes is independent of prominent steroid signaling. Although sex steroid–dependent paracrine factors from neighboring cell populations may influence the dorsal mesenchyme differentiation, we

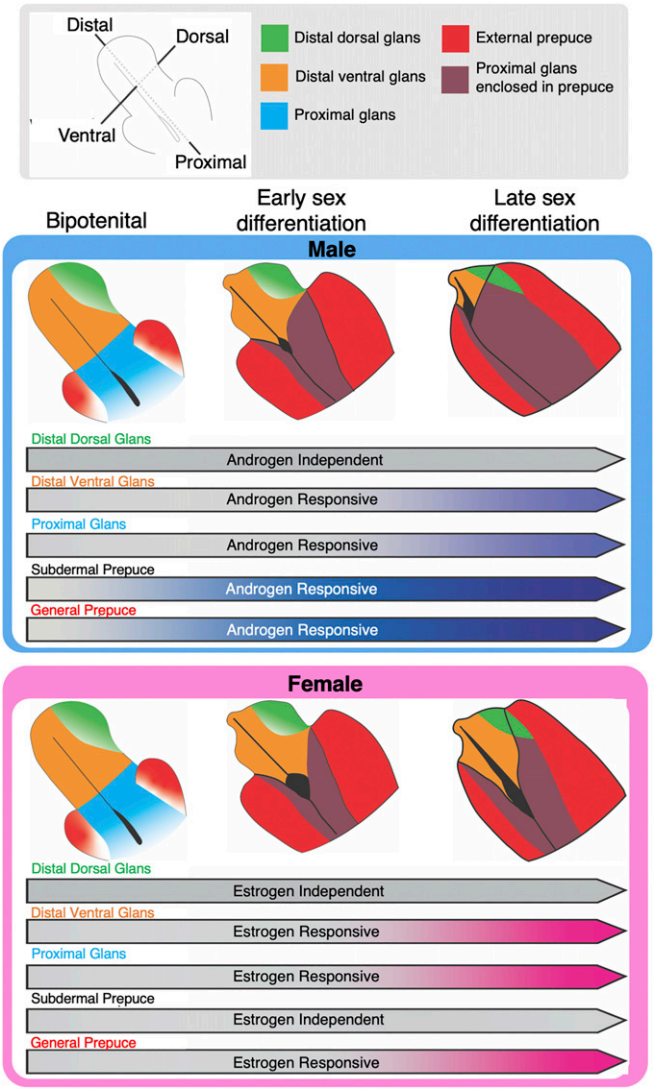

Fig. 7. Model of the sexually dimorphic trajectory of the preputial and glanular mesenchyme cell populations. Tissue-specific morphogenetic events that occur in the male and female genitalia from the bipotential stage, early sexual differentiation, to the late sex differentiation stage. The arrows represent tissue-specific sex steroid response over the developmental stage.

suspect that the dorsal mesenchyme is a site of sex steroid–independent dimorphisms. The sex steroid–independent dimorphisms could be tightly linked to TGF-B signaling based on the presence of *Inhba* and other TGF-B signaling pathways.

Given the prevalence of external genitalia defects throughout the world, understanding how the external genitalia forms is paramount in identifying potential causes for the defect and to develop treatment strategy. The data we provide here are the first step to characterizing and understanding external genitalia formation. Although mice and humans share many similarities in external genitalia formation, some key differences exist and should be considered when interpreting this data. In the mouse, there is the presence of a baculum (80), presence of two prepuces (81), absence of a corpus spongiosum that surrounds the urethra (82), and a unique mechanism of proximal urethra closure (83) that does not occur in the human. Ultimately, the comparison of future human single-cell RNA sequencing data with the mouse single-cell RNA sequencing data will unveil the similarities and differences between mouse and human external genitalia development.

The formation of a functional external genitalia requires the coordinated interaction among multiple cell populations in the embryonic progenitor organ (1). Using single-cell sequencing, we unbiasedly and definitively dissect the external genitalia in distinct cell populations, with a particular focus on the mesenchyme cell populations, which are known to play a major role in external genitalia morphogenesis. This wealth of information not only provides a spatial–temporal atlas that portrays the sexual dimorphism of embryonic external genitalia but also identifies potential candidate genes that may be involved in congenital defects of the external genitalia.

Materials and Methods

Mouse Models. All mice used for single-cell sequencing were of the B6/129 background. Mice were time mated, and the observation of a vaginal plug was defined as E0.5. Female mice were then separated from males. At dissection, the developmental stage was confirmed by the Theiler staging criteria, and mice were sexed by evaluating the presence of testis or ovaries. All animal procedures were approved by the National Institute of Environmental Health Sciences (NIEHS) Animal Care and Use Committee and are in compliance with a NIEHS-approved animal study proposal.

Cell Disassociation and Single-Cell Suspension. External genitalia (n = 2) at E14.5, E16.5, and E18.5 were dissected from the body by extracting the external genitalia at the point where the external genitalia meet the perineum. The genitalia were placed in ice-cold, sterilized 1× phosphate-buffered saline (PBS) and 0.04% bovine serum albumin (BSA) until the dissection of the other embryos were completed. Once completed, a stock solution of disassociation media was made by combining 1× PBS, 0.04% BSA, 1.2 U/mL Dispase II (Roche 04942078001), 1 mg/mL Collagenase IV (Gibco 17104–019), and 5 U/mL deoxyribonuclease I (Roche 1010459001). Next, 1.5-mL centrifuge tubes were filled with 250 μL disassociation stock, and the external genitalia were transferred to tubes. External genitalia were incubated in a VorTemp 56 (Labnet) at 37 °C and 1,000 RPM agitation. After 15 min of agitation, genitalia were mechanically disassociated with a P1000 pipette and incubated at 37 °C for another 5 min. The samples were then mechanically disassociated with a P200 pipette and incubated at 37 °C for another 5 min. The samples were visually inspected to ensure single-cell suspension. A total of 500 μL room temperature 1× PBS with 0.04% BSA was added to the cell suspension to stop the reaction. Cells were spun at 300 × g for 5 min. Supernatant was removed, and cells were resuspended in 100 μL 1× PBS with 0.04% BSA. Cells were kept on ice. Live dead counts were conducted with Trypan Blue (Sigma-Aldrich T8154) on the Bio-Rad TC20. The samples that had a living percentage <80% were not used for future preparation. Cell size histograms and bright-field images were visually assessed to determine whether single suspension was achieved. A target capture of 8,000 cells was loaded into the 10× Chromium instrument (10x Genomics). After single-cell capture, libraries were prepped with Chromium Single Cell 3′ v3.1 Reagent Kit (10x Genomics) following the provided 10x Genomics instruction manual. Two independent biological replicates were used for each sex by developmental stage combination.

Library Preparation, Sequencing, and Sequence Alignments. All libraries were prepared by strictly following the 10x Genomics library preparation protocol. Libraries were pooled into a single tube and sequenced on an Illumina NovaSeq. 6000 sequencer with an S4 flow cell. Libraries were paired-end sequenced with a 26-bp (base pair) first read and a 96-bp second read. The target depth for libraries was 40,000 total reads per cell. Library preparation and sequencing was done at the NIEHS. Data were aligned using default Cell Ranger parameters.

Analysis of Single-Cell Data. Seurat V4.0 was used for all data analysis. All data were uploaded into R v3.6.3 and processed in the same manner. For more detailed information on filtering and gene marker identification, please refer to *SI Appendix, Supplemental Methods*.

RNAscope and Immunofluorescence Validation. Samples for RNAscope and immunofluorescence were preserved in 4% paraformaldehyde overnight at 4 °C, incubated in 20% sucrose overnight, embedded in optimal cutting temperature compound, and sectioned at 10 μM and mounted on Superfrost Plus slides (Fisherbrand, 12–550-15). RNAscope probes *Fst* (553211), *Mfap5* (490211-C3), *Gli1* (311001-C2), *Inhba* (455871-C2), and *Dlx5* (478151-C3) were used on sectioned tissues. RNAscope was conducted according to vendor's protocol. Immunofluorescence was conducted with AKAP12 (anti-rabbit, from Irwin Gelman of Roswell Park Comprehensive Cancer Center, Buffalo, NY) and IRX1 (anti-rabbit, Novus NBP1-83090) antibodies on sectioned samples. Briefly for immunofluorescence, sections were permeabilized in 1× PBS with 0.1% Triton and blocked for 1 h with donkey serum. The primary antibody was incubated on slides at 4 °C overnight. Slides were washed with 1× PBS + 0.1% Triton, and the secondary (donkey-anti-rabbit Alexa Fluor 488) was added and incubated for 2 h. Slides were imaged the day after processing.

Data Availability. All single-cell RNA sequencing data are deposited and available on the Gene Expression Omnibus (accession no. GSE174712). All R scripts used to analyze data are available in Code S1.

ACKNOWLEDGMENTS. We thank Dr. Xin Xu and Brian Papas (Epigenomics and DNA Sequencing Core Facility and Integrative Bioinformatics Support Group in the NIEHS) for help with single-cell library preparation, initial data filtering, and barcode identification, Dr. Bevin Blake (Environmental Protection Agency) for reviewing and providing critical feedback for our manuscript, Dr. Oswaldo Lozoya (NIEHS) for insightful conversations and critical feedback, and Drs. Karina Rodriguez and Barbara Nicol for their extensive help on a variety of aspects in this project (NIEHS). We also thank Dr. Irwin Gelman (Roswell Park Comprehensive Cancer Center) for the AKAP12 antibody. We thank Diane Bailey (Comparative Medicine Branch) for her expertise in animal husbandry. This work was supported by the Intramural Research Program (Grant Z01 ES102965 to H.H.-C.Y.) of the NIH, NIEHS.

1. K. M. Georgas *et al.*, An illustrated anatomical ontology of the developing mouse lower urogenital tract. *Development* **142**, 1893–1908 (2015).
2. M. Haller, L. Ma, Temporal, spatial, and genetic regulation of external genitalia development. *Differentiation* **110**, 1–7 (2019).
3. L. J. Paulozzi, J. D. Erickson, R. J. Jackson, Hypospadias trends in two US surveillance systems. *Pediatrics* **100**, 831–834 (1997).
4. X. Yu *et al.*, Hypospadias prevalence and trends in international birth defect surveillance systems, 1980-2010. *Eur. Urol.* **76**, 482–490 (2019).
5. Z. Zheng, B. A. Armfield, M. J. Cohn, Timing of androgen receptor disruption and estrogen exposure underlies a spectrum of congenital penile anomalies. *Proc. Natl. Acad. Sci. U.S.A.* **112**, E7194–E7203 (2015).
6. L. C. Govers *et al.*, A critical role for estrogen signaling in penis development. *FASEB J.* **33**, 10383–10392 (2019).
7. J. H. Yang, J. Menshenina, G. R. Cunha, N. Place, L. S. Baskin, Morphology of mouse external genitalia: Implications for a role of estrogen in sexual dimorphism of the mouse genital tubercle. *J. Urol.* **184** (suppl. 4), 1604–1609 (2010).
8. C. M. Amato, M. Boyd, J. Yang, K. A. McCoy, Organizational effects of the anti-androgen, vinclozolin, on penis development in the mouse. *Biol. Reprod.* **99**, 639–649 (2018).
9. M. Welsh, D. J. MacLeod, M. Walker, L. B. Smith, R. M. Sharpe, Critical androgen-sensitive periods of rat penis and clitoris development. *Int. J. Androl.* **33**, e144–e152 (2010).
10. H. Chen *et al.*, Fkbp52 regulates androgen receptor transactivation activity and male urethra morphogenesis. *J. Biol. Chem.* **285**, 27776–27784 (2010).
11. H. O. Goyal *et al.*, Estrogen receptor alpha mediates estrogen-inducible abnormalities in the developing penis. *Reproduction* **133**, 1057–1067 (2007).
12. H. O. Goyal, T. D. Braden, C. S. Williams, J. W. Williams, Estrogen-induced developmental disorders of the rat penis involve both estrogen receptor (ESR)- and androgen receptor (AR)-mediated pathways. *Biol. Reprod.* **81**, 507–516 (2009).
13. H. J. van der Horst, L. L. de Wall, Hypospadias, all there is to know. *Eur. J. Pediatr.* **176**, 435–441 (2017).
14. L. Ságodi, A. Kiss, E. Kiss-Tóth, L. Barkai, Prevalence and possible causes of hypospadias [in Hu]. *Orv. Hetil.* **155**, 978–985 (2014).

15. L. A. Ipulan *et al*., Development of the external genitalia and their sexual dimorphic regulation in mice. *Sex Dev.* **8**, 297–310 (2014).
16. R. Satija, J. A. Farrell, D. Gennert, A. F. Schier, A. Regev, Spatial reconstruction of single-cell gene expression data. *Nat. Biotechnol.* **33**, 495–502 (2015).
17. E. Becht *et al*., Dimensionality reduction for visualizing single-cell data using UMAP. *Nat. Biotechnol.*, 10.1038/nbt.4314 (2018).
18. S. Millington-Ward *et al*., RNAi of COL1A1 in mesenchymal progenitor cells. *Eur. J. Hum. Genet.* **12**, 864–866 (2004).
19. A. Abedini, C. Sayed, L. E. Carter, D. Boerboom, B. C. Vanderhyden, Non-canonical WNT5a regulates epithelial-to-mesenchymal transition in the mouse ovarian surface epithelium. *Sci. Rep.* **10**, 9695 (2020).
20. Q. Q. Zhu, C. Ma, Q. Wang, Y. Song, T. Lv, The role of TWIST1 in epithelial-mesenchymal transition and cancers. *Tumour Biol.* **37**, 185–197 (2016).
21. D. Vestweber; V. D, VE-cadherin: The major endothelial adhesion molecule controlling cellular junctions and blood vessel formation. *Arterioscler. Thromb. Vasc. Biol.* **28**, 223–232 (2008).
22. J. R. Privratsky, P. J. Newman, PECAM-1: Regulator of endothelial junctional integrity. *Cell Tissue Res.* **355**, 607–619 (2014).
23. S. Pinte *et al*., Endothelial cell activation is regulated by epidermal growth factor-like domain 7 (Egfl7) during inflammation. *J. Biol. Chem.* **291**, 24017–24028 (2016).
24. W. Han, C. Hu, Z. J. Fan, G. L. Shen, Transcript levels of keratin 1/5/6/14/15/16/17 as potential prognostic indicators in melanoma patients. *Sci. Rep.* **11**, 1023 (2021).
25. J. Shi, L. Hua, D. Harmer, P. Li, G. Ren, Cre driver mice targeting macrophages. *Methods Mol. Biol.* **1784**, 263–275 (2018).
26. I. G. De Plaen *et al*., Lipopolysaccharide induces CXCL2/macrophage inflammatory protein-2 gene expression in enterocytes via NF-kappaB activation: Independence from endogenous TNF-alpha and platelet-activating factor. *Immunology* **118**, 153–163 (2006).
27. K. C. El Kasmi *et al*., Macrophage-derived IL-1β/NF-κB signaling mediates parenteral nutrition-associated cholestasis. *Nat. Commun.* **9**, 1393 (2018).
28. S. Colombo, D. Champeval, F. Rambow, L. Larue, Transcriptomic analysis of mouse embryonic skin cells reveals previously unreported genes expressed in melanoblasts. *J. Invest. Dermatol.* **132**, 170–178 (2012).
29. M. Takeo *et al*., EdnrB governs regenerative response of melanocyte stem cells by crosstalk with Wnt signaling. *Cell Rep.* **15**, 1291–1302 (2016).
30. D. C. Guo *et al*., Mutations in smooth muscle alpha-actin (ACTA2) lead to thoracic aortic aneurysms and dissections. *Nat. Genet.* **39**, 1488–1493 (2007).
31. H. Obata *et al*., Smooth muscle cell phenotype-dependent transcriptional regulation of the alpha1 integrin gene. *J. Biol. Chem.* **272**, 26643–26651 (1997).
32. J. Li *et al*., Regulator of G protein signaling 5 marks peripheral arterial smooth muscle cells and is downregulated in atherosclerotic plaque. *J. Vasc. Surg.* **40**, 519–528 (2004).
33. C. P. Sommerhoff *et al*., Mast cell chymase: A potent secretagogue for airway gland serous cells. *J. Immunol.* **142**, 2450–2456 (1989).
34. T. Takabayashi *et al*., Glandular mast cells with distinct phenotype are highly elevated in chronic rhinosinusitis with nasal polyps. *J. Allergy Clin. Immunol.* **130**, 410–20.e5 (2012).
35. J. J. Wang *et al*., Isl-1 positive pharyngeal mesenchyme subpopulation and its role in the separation and remodeling of the aortic sac in embryonic mouse heart. *Dev. Dyn.* **248**, 771–783 (2019).
36. D. R. Archambeault, J. Tomaszewski, A. Joseph, B. T. Hinton, H. H. Yao, Epithelial-mesenchymal crosstalk in Wolffian duct and fetal testis cord development. *Genesis* **47**, 40–48 (2009).
37. L. Landsman *et al*., Pancreatic mesenchyme regulates epithelial organogenesis throughout development. *PLoS Biol.* **9**, e1001143 (2011).
38. E. D. Hay, The mesenchymal cell, its role in the embryo, and the remarkable signaling mechanisms that create it. *Dev. Dyn.* **233**, 706–720 (2005).
39. K. Suzuki *et al*., Sexually dimorphic expression of Mafb regulates masculinization of the embryonic urethral formation. *Proc. Natl. Acad. Sci. U.S.A.* **111**, 16407–16412 (2014).
40. L. Liu *et al*., Androgen regulates dimorphic F-actin assemblies in the genital organogenesis. *Sex Dev.* **11**, 190–202 (2017).
41. E. A. Morgan, S. B. Nguyen, V. Scott, H. S. Stadler, Loss of Bmp7 and Fgf8 signaling in Hoxa13-mutant mice causes hypospadia. *Development* **130**, 3095–3109 (2003).
42. R. Sreenivasan *et al*., Altered SOX9 genital tubercle enhancer region in hypospadias. *J. Steroid Biochem. Mol. Biol.* **170**, 28–38 (2017).
43. A. M. Herrera, S. G. Shuster, C. L. Perriton, M. J. Cohn, Developmental basis of phallus reduction during bird evolution. *Curr. Biol.* **23**, 1065–1074 (2013).
44. K. M. Vasudevan, S. Gurumurthy, V. M. Rangnekar, Suppression of PTEN expression by NF-kappa B prevents apoptosis. *Mol. Cell. Biol.* **24**, 1007–1021 (2004).
45. S. E. Beck, J. M. Carethers, BMP suppresses PTEN expression via RAS/ERK signaling. *Cancer Biol. Ther.* **6**, 1313–1317 (2007).
46. H. Zhao, J. Dupont, S. Yakar, M. Karas, D. LeRoith, PTEN inhibits cell proliferation and induces apoptosis by downregulating cell surface IGF-IR expression in prostate cancer cells. *Oncogene* **23**, 786–794 (2004).
47. S. Miyagawa *et al*., Genetic interactions of the androgen and Wnt/beta-catenin pathways for the masculinization of external genitalia. *Mol. Endocrinol.* **23**, 871–880 (2009).
48. Y. Zhou *et al*., Epithelial-mesenchymal transformation and apoptosis in rat urethra development. *Pediatr. Res.* **82**, 1073–1079 (2017).
49. V. Rothhammer, F. J. Quintana, The aryl hydrocarbon receptor: An environmental sensor integrating immune responses in health and disease. *Nat. Rev. Immunol.* **19**, 184–197 (2019).
50. X. Y. Qin *et al*., Association of variants in genes involved in environmental chemical metabolism and risk of cryptorchidism and hypospadias. *J. Hum. Genet.* **57**, 434–441 (2012).
51. Q. Ma, Role of nrf2 in oxidative stress and toxicity. *Annu. Rev. Pharmacol. Toxicol.* **53**, 401–426 (2013).
52. A. T. Nurden, Clinical significance of altered collagen-receptor functioning in platelets with emphasis on glycoprotein VI. *Blood Rev.* **38**, 100592 (2019).
53. M. F. O'Leary, G. R. Wallace, A. J. Bennett, K. Tsintzas, S. W. Jones, IL-15 promotes human myogenesis and mitigates the detrimental effects of TNFα on myotube development. *Sci. Rep.* **7**, 12997 (2017).
54. C. Xu, C. Y. Li, A. N. Kong, Induction of phase I, II and III drug metabolism/transport by xenobiotics. *Arch. Pharm. Res.* **28**, 249–268 (2005).
55. M. L. Ruehr *et al*., Targeting of protein kinase A by muscle A kinase-anchoring protein (mAKAP) regulates phosphorylation and function of the skeletal muscle ryanodine receptor. *J. Biol. Chem.* **278**, 24831–24836 (2003).
56. L. Baskin *et al*., Androgen and estrogen receptor expression in the developing human penis and clitoris. *Differentiation* **111**, 41–59 (2020).
57. S. Wang, J. Lawless, Z. Zheng, Prenatal low-dose methyltestosterone, but not dihydrotestosterone, treatment induces penile formation in female mice and Guinea pigs. *Biol. Reprod.* **102**, 1248–1260 (2020).
58. A. O. Brinkmann *et al*., Mechanisms of androgen receptor activation and function. *J. Steroid Biochem. Mol. Biol.* **69**, 307–313 (1999).
59. C. Tohyama *et al*., Testosterone-dependent induction of metallothionein in genital organs of male rats. *Biochem. J.* **317**, 97–102 (1996).
60. M. S. Mahendroo, K. M. Cala, D. L. Hess, D. W. Russell, Unexpected virilization in male mice lacking steroid 5 alpha-reductase enzymes. *Endocrinology* **142**, 4652–4662 (2001).
61. L. A. Okumu, T. D. Braden, K. Vail, L. Simon, H. O. Goyal, Low androgen induced penile maldevelopment involves altered gene expression of biomarkers of smooth muscle differentiation and a key enzyme regulating cavernous smooth muscle cell tone. *J. Urol.* **192**, 267–273 (2014).
62. L. Eklund *et al*., Lack of type XV collagen causes a skeletal myopathy and cardiovascular defects in mice. *Proc. Natl. Acad. Sci. U.S.A.* **98**, 1194–1199 (2001).
63. T. Shimizu *et al*., Actions and interactions of progesterone and estrogen on transcriptome profiles of the bovine endometrium. *Physiol. Genomics* **42A**, 290–300 (2010).
64. D. R. Boverhof, L. D. Burgoon, K. J. Williams, T. R. Zacharewski, Inhibition of estrogen-mediated uterine gene expression responses by dioxin. *Mol. Pharmacol.* **73**, 82–93 (2008).
65. J. Eeckhoute *et al*., Positive cross-regulatory loop ties GATA-3 to estrogen receptor alpha expression in breast cancer. *Cancer Res.* **67**, 6477–6483 (2007).
66. T. R. Phillips, D. K. Wright, P. E. Gradie, L. A. Johnston, A. J. Pask, A comprehensive atlas of the adult mouse penis. *Sex Dev.* **9**, 162–172 (2015).
67. E. Padilla-Banks, W. N. Jefferson, P. H. Myers, D. R. Goulding, C. J. Williams, Neonatal phytoestrogen exposure causes hypospadias in female mice. *Mol. Reprod. Dev.* **79**, 3 (2012).
68. L. S. Baskin *et al*., Urethral seam formation and hypospadias. *Cell Tissue Res.* **305**, 379–387 (2001).
69. S. A. Gilpin, J. A. Gosling, Smooth muscle in the wall of the developing human urinary bladder and urethra. *J. Anat.* **137**, 503–512 (1983).
70. M. A. B. Fahmy, *Normal and Abnormal Prepuce* (Springer, 2020).
71. C. L. Dearth *et al*., Skeletal muscle cells express ICAM-1 after muscle overload and ICAM-1 contributes to the ensuing hypertrophic response. *PLoS One* **8**, e58486 (2013).
72. Y. A. Goo *et al*., Stromal mesenchyme cell genes of the human prostate and bladder. *BMC Urol.* **5**, 17 (2005).
73. C. J. Cold, J. R. Taylor, The prepuce. *BJU Int.* **83** (suppl. 1), 34–44 (1999).
74. K. Suzuki *et al*., Regulation of outgrowth and apoptosis for the terminal appendage: External genitalia development by concerted actions of BMP signaling [corrected]. *Development* **130**, 6209–6220 (2003).
75. C. W. Brown, D. E. Houston-Hawkins, T. K. Woodruff, M. M. Matzuk, Insertion of Inhbb into the Inhba locus rescues the Inhba-null phenotype and reveals new activin functions. *Nat. Genet.* **25**, 453–457 (2000).
76. S. Y. Ying, Inhibins and activins: Chemical properties and biological activity. *Proc. Soc. Exp. Biol. Med.* **186**, 253–264 (1987).
77. S. Botta, G. R. Cunha, L. S. Baskin, Do endocrine disruptors cause hypospadias? *Transl. Androl. Urol.* **3**, 330–339 (2014).
78. S. Matsushita *et al*., Regulation of masculinization: Androgen signalling for external genitalia development. *Nat. Rev. Urol.* **15**, 358–368 (2018).
79. G. R. Cunha *et al*., Androgen-independent events in penile development in humans and animals. *Differentiation* **111**, 98–114 (2020).
80. N. G. Schultz, M. Lough-Stevens, E. Abreu, T. Orr, M. D. Dean, The baculum was gained and lost multiple times during mammalian evolution. *Integr. Comp. Biol.* **56**, 644–656 (2016).
81. S. D. Blaschko *et al*., Analysis of the effect of estrogen/androgen perturbation on penile development in transgenic and diethylstilbestrol-treated mice. *Anat. Rec. (Hoboken)* **296**, 1127–1141 (2013).
82. E. Rodriguez Jr *et al*., New insights on the morphology of adult mouse penis. *Biol. Reprod.* **85**, 1216–1221 (2011).
83. G. Liu *et al*., Contrasting mechanisms of penile urethral formation in mouse and human. *Differentiation* **101**, 46–64 (2018).